



Comparison of bone microstructure and strength in the distal radius and tibia between the different types of primary hypertrophic osteoarthropathy: an HR-pQCT study

Qianqian Pang¹ · Yuping Xu¹ · Ruoxi Liao¹ · Ye Li² · Li Zhang¹ · Yue Chi¹ · Xuan Qi¹ · Mei Li¹ · Yan Jiang¹ · Ou Wang¹ · Xiaoping Xing¹ · Ling Qin² · Weibo Xia¹ 

Received: 20 September 2022 / Accepted: 1 May 2023 / Published online: 18 May 2023

© The Author(s) 2023

Abstract

Summary Primary hypertrophic osteoarthropathy (PHO) is a hereditary bone disease that is grouped into PHO autosomal recessive 1 (PHOAR1) and PHO autosomal recessive 2 (PHOAR2) due to different causative genes. Data comparing bone microstructure between the two subtypes are scarce. This is the first study to find that PHOAR1 patients had inferior bone microstructure compared with PHOAR2 patients.

Purpose The primary goal of this study was to assess bone microarchitecture and strength in PHOAR1 and PHOAR2 patients and to compare them with age- and sex-matched healthy controls (HCs). The secondary goal was to assess the differences between PHOAR1 and PHOAR2 patients.

Methods Twenty-seven male Chinese PHO patients (PHOAR1 = 7; PHOAR2 = 20) were recruited from Peking Union Medical College Hospital. The areal bone mineral density (aBMD) was assessed by dual-energy X-ray absorptiometry (DXA). Peripheral bone microarchitecture at the distal radius and tibia were evaluated by high-resolution peripheral quantitative computed tomography (HR-pQCT). Biochemical markers of PGE2, bone turnover, and Dickkopf-1 (DKK1) were investigated.

Results Compared with HCs, PHOAR1 and PHOAR2 patients had distinctively larger bone geometry, substantially lower vBMD at the radius and tibia, and compromised cortical microstructure at the radius. For trabecular bone, PHOAR1 and PHOAR2 patients showed different changes at the tibia. PHOAR1 patients had significant deficits in the trabecular compartment, resulting in lower estimated bone strength. Conversely, PHOAR2 patients showed a higher trabecular number, narrower trabecular separation, and lower trabecular network inhomogeneity than HCs, translating into preserved or slightly high estimated bone strength.

Conclusion PHOAR1 patients had inferior bone microstructure and strength compared with PHOAR2 patients and HCs. Additionally, this study was the first to find differences in the bone microstructure between PHOAR1 and PHOAR2 patients.

Keywords DKK1 · HR-pQCT · PHO · PHOAR1 · PHOAR2

✉ Ling Qin
lingqin@cuhk.edu.hk

✉ Weibo Xia
xiaweibo8301@163.com

¹ Department of Endocrinology, Key Laboratory of Endocrinology, State Key Laboratory of Complex Severe and Rare Diseases, NHC, Peking Union Medical College Hospital, Chinese Academy of Medical Sciences, Beijing 100730, China

² Musculoskeletal Research Laboratory and Bone Quality and Health Assessment Centre, Department of Orthopedics & Traumatology, The Chinese University of Hong Kong, Prince of Wales Hospital, 5/F Lui Che Woo Clinical Sciences Building Shatin, N.T., Hong Kong SAR, Hong Kong

Introduction

Primary hypertrophic osteoarthropathy (PHO: MIM: 167,100) is a hereditary bone disease mainly characterized by a distinctive trait: periostosis, pachydermia, finger clubbing, and joint swelling. PHO was first reported by Friedreich in 1868 [1]. The pathogenesis and inherited pattern were controversial until Uppal et al. identified that mutations in the hydroxyprostaglandin dehydrogenase (*HPGD*) gene, which encodes 15-hydroxyprostaglandin dehydrogenase (15-PGDH), a prostaglandin E2 (PGE2) degradation enzyme, could be responsible for PHO autosomal recessive 1 (PHOAR1: MIM: 259,100, 2008) [2]. Subsequently, another

pathogenic gene, *SLCO2A1*, which encodes the prostaglandin transporter (PGT) responsible for the uptake of PGE₂, was found to be the cause of PHO autosomal recessive 2 (PHOAR2: MIM: 614,441, 2012) [3]. Both genetic studies point to the same factor, i.e., PGE₂. Biochemical analyses in PHO patients indicated the critical role of disturbed PGE₂ catabolism, which leads to elevated circulating PGE₂ levels, in the pathogenesis in both PHOAR1 and PHOAR2 patients [4, 5].

PGE₂ is a critical mediator of several physiologic and pathologic processes. PGE₂ level in the two forms of PHO patients was found to have remarkable differences. In Li et al.'s study, PGE₂ levels were significantly higher in PHOAR2 patients than in PHOAR1 patients [6]. In our previous study, the serum and urinary PGE₂ metabolites (PGEM) in PHOAR2 patients were also found to be much higher than those in PHOAR1 patients [7]. Significant differences in phenotypes between the two forms of PHO were suggested by some studies, including onset age, pachydermia, joint pain, and gastrointestinal hemorrhage [6, 7]. PGE₂ is well known to activate both osteoclasts and osteoblasts [8]. In in vivo studies, PGE₂ was reported to mainly affect bone structure and strength. Our previous studies reported alterations in bone microstructure either in distal interphalangeal joints (short bones) or distal tibia (long bones) in PHO patients (PHOAR1 patients and PHOAR2 patients) using high-resolution peripheral quantitative computed tomography (HR-pQCT) [9, 10]. None of the above study PHO patients had fractures. PGE₂ levels were closely related to alterations in bone microstructure parameters, indicating the critical role of PGE₂ in alterations in bone microstructure in PHO patients [9, 10]. However, whether there were differences in bone structure and bone density due to the variety of PGE₂ levels between the two forms of PHO patients remains unclear.

Wingless-type (Wnt) signaling is central to bone development and homeostasis. Dickkopf-1 (DKK1) is the osteocyte-produced protein that antagonizes Wnt signaling in osteoblasts, leading to inhibition of osteoblast differentiation and bone formation in humans. Our previous study showed typical periostosis imaging features with general and symmetrical periostosis in the cortex of the tibia in PHO patients, indicating high rates of bone formation in PHO patients [10]. However, the mechanism of abnormal bone formation in PHO patients has yet to be fully elucidated. Studies have reported that haploinsufficiency of DKK1 increases Wnt activity and results in a high bone mass phenotype because of higher rates of bone formation [11, 12]. We thus hypothesized that DKK1 could play a role in abnormalities of bone formation in PHO patients, leading to remarkable periostosis and osteophytes.

Here, we reported 7 unrelated male Chinese PHOAR1 patients and 20 unrelated Chinese PHOAR2 patients,

of which 20 were previously reported [10]. This study is aimed at (1) determining bone microarchitecture and bone strength, measured by HR-pQCT, in the two subtypes of PHO patients compared to healthy controls; (2) assessing PGE₂ levels, bone turnover markers, DKK1, bone mineral density (BMD), microarchitecture, and bone strength and revealing the differences in these parameters between the two subtypes; and (3) investigating the role of PGE₂ levels, bone turnover marker levels, and DKK1 levels in the BMD, microarchitecture, and bone strength differences of the two subtypes of PHO patients.

Methods and materials

Subjects

The study protocol was approved by the Ethics Committee of Peking Union Medical College Hospital (PUMCH) (zs-1115). After receiving a full explanation of the purpose of the study, all participants signed informed consent documents. Medical history was collected by retrospective review of medical records and clinical inquiry. X-ray radiography of the legs was analyzed. Areal BMD (aBMD) of the lumbar spine and proximal femur were collected (Prodigy Advance; GE Lunar Corporation, Madison, WI, USA). Genomic DNA was extracted from the peripheral white blood cells of the patients for *HPGD* and *SLCO2A1* mutation analysis. Seven male PHO patients were diagnosed based on clinical, radiological, and genetic criteria from 2019 to 2021. Our previous study described PHO patients' inclusion and exclusion criteria in detail [10]. Another 20 male PHO patients reported in our previous study were also included in this study [10]. Twenty-seven PHO patients with definitive clinical and genetic diagnoses in our center were included for comparison between PHOAR1 and PHOAR2 patients.

HR-pQCT scans were performed in age- and sex-matched healthy controls (HCs, $n = 27$). HCs were drawn from an HR-pQCT database of a previous study that collected a population of 249 healthy adult men to establish HR-pQCT reference parameters in the Chinese population [13].

Biochemistry

Blood samples and 24 h urine were drawn after an overnight fast for biochemistry measurements. The Roche electrochemiluminescence system measured beta-C-telopeptides of type I collagen (β -CTX) (E170, Roche Diagnostics, Basel, Switzerland). Serum-free soluble receptor activator of nuclear factor-kappaB ligand (sRANK), osteoprotegerin (OPG), and DKK1 were measured by an enzyme-linked immunosorbent assay (ELISA) using standard kits (Human sRANKL (Total), Human osteoprotegerin, Biovendor, Brno,

Czech Republic; Human DKK-1 Quantikine, R&D Systems). Urinary PGE2 and PGEM levels were measured by competitive ELISA using standard kits (Cayman Chemicals, Ann Arbor, Michigan, USA). All biochemical parameters were evaluated in PHO patients. Simultaneously, DKK1, sRANKL, and OPG were assessed in HCs.

HR-pQCT

We scanned the non-dominant distal radius and distal tibia in all PHO patients and HCs using an HR-pQCT system (Xtreme CTII, Scanco Medical AG, Brüttisellen, Switzerland). Each image was composed of 168 slices with an isotropic resolution of 61 μm . The scan region was positioned 9.0 mm and 22.0 mm proximal to the reference line for the distal radius and distal tibia, respectively. At the time of acquisition, image quality was scored after image reconstruction by two of the authors (PQQ and XYP) using a visual grading system as suggested by published studies [10, 14]. Briefly, grade 1 has no visible artifacts; grade 2 has visible artifacts with no discontinuities in the cortical shell but a small streak in the soft tissue; grade 3 has visible artifacts with no discontinuities in the cortical shell but a medium-large streak in the soft tissue; grade 4 and grade 5 have visible artifacts with both discontinuities and streaks [10, 14]. After evaluation, images with a manual grade of 4 or higher were deemed insufficient quality and excluded.

Image analysis was performed according to the manufacturers' standard in vivo acquisition protocols [13]. "Trabecularization" of cortical bone is the typical image feature in PHO patients with irregular and spiculated periosteosis widely around the cortical bone. Automatically generated contours by built-in software might lead to greater accuracy errors arising in the segmentation of cortical and trabecular bone, resulting in a systematic bias with certain parameters, such as cortical density and thickness. To better define the cortical and trabecular compartments of the PHOAR1 and PHOAR2 patients in this study, a snake algorithm (v5.42, Scanco Medical) was used to generate the periosteal contour and corrected manually as our previous study recommendation. Briefly, cases with cortical fragmentations and periosteal contour retracts were manually corrected. Bone fragments was identified as the sharp bone outside the cortical bone surface but adherent to the cortical bone surface. For the bone fragments analysis, distal tibia and radius were evaluated on a PACS workstation using the open source Digital Imaging and Communication in Medicine (DICOM) OsiriX software (OsiriX MD 10.0; download from www.osirix-viewer.com). As there were no standard protocols for defining the volume of the bone fragments of PHO patients, we measured the volume of the bone fragments using a semi-automated method. The area of a bone fragment was determined by defining the entire area of the

distal tibia on each image of the bone fragment (A1) or excluding the bone fragment (A2). The volume of the bone fragment (V_b) was calculated as $V_b = (A1 - A2) \times n \times 0.061$, in which n is the total number of slices with the bone fragments and 0.061 is the height of the slice. Finally, the average volume of bone fragments in a PHO patient was V_b/N_b , in which N_b is the total number of bone fragments in a PHO patient. PHOAR1 patients' mean of the bone fragments volume was $2.07 \pm 0.78 \text{mm}^3$ ($0.51 \sim 4.12 \text{mm}^3$) in distal tibia and was $1.53 \pm 0.36 \text{mm}^3$ ($0.25 \sim 2.98 \text{mm}^3$) in distal radius. PHOAR2 patients' mean of the bone fragments volume was $2.73 \pm 1.03 \text{mm}^3$ ($0.38 \sim 5.63 \text{mm}^3$) in distal tibia and $1.96 \pm 0.25 \text{mm}^3$ ($0.14 \sim 3.21 \text{mm}^3$) in distal radius. There was no significant bone fragment volume difference between PHOAR1 and PHOAR2 patients. And then, the HR-pQCT images were analyzed twice, including bone fragments or excluding bone fragments, to confirm whether the bone fragments could influence the density and bone strength. Supplementary Table 1 shows no significant differences in HR-pQCT parameters and mechanical properties between the two groups with or without bone fragments. Cases with spiculated periosteosis (sharp bone fragments outside the cortical bone surface) that protrude to a certain extent from the periosteal surface of the cortex were excluded from the cortical contours [10].

The following parameters were calculated directly and reported automatically [15]: (1) total bone mineral density (Tt.BMD), cortical bone mineral density (Ct.BMD), and trabecular bone mineral density (Tb.BMD) which were derived from their respective volumes and expressed in mg hydroxyapatite (mg/cm^3); (2) total, trabecular, and cortical bone cross-sectional area, respectively (Tt.Ar, Tb.Ar, and Ct.Ar; mm^2); (3) trabecular microstructure, including trabecular bone volume fraction (Tb.BV/TV), trabecular number (Tb.N, 1/mm), trabecular thickness (Tb.Th, mm), trabecular separation (Tb.Sp, mm), and inhomogeneity of the trabecular network (Tb.1/N.SD, tmm) (structure model index (SMI) measured rods and plates in trabecular bone; studies have suggested that plate structures have greater mechanical strength than rod structures [16, 17]); and (4) cortical microstructure, including cortical porosity (Ct.Po, %), cortical thickness (Ct.Th, mm), and cortical perimeter (Ct.Pm, mm).

Finite element analysis (FEA) was used to estimate the failure load in compression, wherein all bone materials were given a Young's modulus of 10.0 GPa and a Poisson's ratio of 0.3. All FEA was performed using FE-solver included in the built-in Image Processing Language software (vision 1.13, Finite Element Analysis software, Scanco Medical). The following are the primary outcomes of mechanical properties: stiffness (kN/mm), apparent modulus (E_a , kN/mm^2), and estimated failure load (FL, kN) [13, 15].

Statistical analysis

Statistical analysis was performed using SPSS version 22.0. Data are presented as the mean \pm standard deviation (SD) or median (interquartile range (IQR)), as appropriate. We assessed the distribution of each demographic parameter for PHO patients, PHOAR1 patients, PHOAR2 patients, and HCs via normality plots and the Shapiro Wilks W test and compared the two groups using Student's t test or the Mann–Whitney U test, as appropriate. Clinical features and biochemical data for PHOAR1 and PHOAR2 patients were compared using Student's t test or Mann–Whitney U test, depending on the type and distribution of the data. Densitometric, geometric, microstructural, and biomechanical indices among the PHOAR1 patients, PHOAR2 patients, and healthy controls were compared using ANOVA with Bonferroni-corrected pairwise comparisons. The predictive effects of disease features and biochemical markers on HR-pQCT parameters for subjects with PHO were evaluated in linear regression models at the radius and the tibia as dependent variables. In addition to the univariate models with disease features and biochemical markers as independent variables, multivariable models adjusting for the type of PHO were considered. Differences with p values less than 0.05 were considered statistically significant.

Results

Basic characteristics

This study recruited 27 patients clinically and genetically diagnosed with PHO and 27 age- and sex-matched HCs. According to the different pathogenic genes, the 27 PHO patients were divided into PHOAR1 and PHOAR2 subgroups: PHOAR1 patients ($n=7$) resulting from *HSPGD* mutations and PHOAR2 patients ($n=20$) due to *SLCO2A1* mutations. All of the participants were male. The demographic characteristics of the study participants are shown in Table 1. PHO patients, PHOAR1 patients, PHOAR2 patients, and HCs were comparable according to age, body weight, and height. The median age of onset in PHOAR1 patients was 1 year old, which was earlier than that in PHOAR2 patients, whose median onset age was 16 years ($p < 0.001$). Hence, the mean disease duration of PHOAR2 was shorter than that of PHOAR1 (9.0 ± 5.7 versus 28.1 ± 8.2 , $p < 0.001$).

Clinical and biochemical characteristics of PHOAR1 and PHOAR2 patients

The clinical characteristics and main biochemical parameters in PHOAR1 and PHOAR2 patients at the time of diagnosis are listed in Table 2. The clinical phenotypes

Table 1 Demographic characteristics of patients with PHO and Healthy controls

Variable	PHO	PHOAR1	PHOAR2	HCs
No. of patients	27	7	20	27
Age (y)	27.0 (9.0)	27.0 (12.0)	27.0 (13.0)	26.7 (3.0)
Height (m)	1.75 (0.04)	1.74 (0.06)	1.75 (0.07)	1.71 (0.05)
Weight (kg)	61.7 \pm 9.7	59.1 \pm 7.8	62.6 \pm 10.3	66.5 \pm 8.2
Onset age (y)	16.0 (11.0)	1.0 (4.0)	16.0 (4.0)***	-
Disease duration (y)	14.0 \pm 10.6	28.1 \pm 8.2	9.0 \pm 5.7***	-

HC healthy controls

Data are expressed as the mean \pm SD or median (interquartile range (IQR))

*** Significant differences to PHOAR1 ($p < 0.001$)

varied between the two subgroups of PHO patients. Seven PHOAR1 patients were diagnosed with complete clinical forms featuring periosteosis, pachydermia, and digital clubbing. Sixteen PHOAR2 patients were diagnosed with complete clinical forms, and another 4 PHOAR2 patients were diagnosed with incomplete clinical forms who lacked the clinical signs of pachydermia.

The medium urinary PGE2/PGEM levels were notably higher in PHOAR1 than in PHOAR2. Regarding age-specific bone turnover markers in healthy Chinese subjects, serum levels of β -CTX, and the sRANKL/OPG ratio in most PHOAR1 and PHOAR2 patients were above the age-related established reference range. DKK1 levels in PHOAR1 and PHOAR2 patients were lower than the normal reference range. Moreover, PHOAR2 patients showed significantly higher β -CTX and DKK1 levels than PHOAR1 patients (all $p < 0.05$ after age, height, and weight correction) (Table 2).

DXA

Six PHOAR1 patients and 19 PHOAR2 patients received dual energy X-ray absorptiometry (DXA) at the lumbar spine and proximal femur. The aBMD values of PHOAR1 and PHOAR2 were all within the normal range. Further subgroup analysis found that no significant differences in aBMD L1-4 were found at the lumbar spine (g/cm^2 , 1.09 ± 0.17 versus 1.19 ± 0.15 and Z-score, -0.13 ± 0.68 versus 1.17 ± 1.36) between PHOAR1 and PHOAR2 patients. aBMD of the femoral neck (g/cm^2 , 0.89 ± 0.16 versus 1.06 ± 0.12 , $p = 0.008$ and Z-score, -0.87 ± 0.65 versus 1.09 ± 1.39 , $p = 0.002$) and aBMD of the total hip (g/cm^2 , 0.88 ± 0.15 versus 1.15 ± 0.16 , $p = 0.001$ and Z-score, -0.12 ± 0.62 versus 1.52 ± 1.29 , $p = 0.001$) were significantly lower in PHOAR1 patients than in PHOAR2 patients (Fig. 1).

Table 2 Comparisons of clinical features and biochemical data at diagnosis between PHOAR1 and PHOAR2 patients

Variables	PHOAR1 (n=7)	PHOAR2 (n=20)	p value
Periosteosis	7	20	–
Pachydermia	7	16	–
Digital clubbing	7	20	–
Urinary PGE2 (ng/mmol Cr)	522.44 (1386.79)	289.57 (787.40)	0.471
Urinary PGE2/PGEM**	70.50 (117.27)	1.75 (2.31)	0.004
β -CTX (ng/mL)*	0.67 \pm 0.10	1.28 \pm 0.99	0.011
sRANKL/OPG	198.62 \pm 101.25	309.87 \pm 172.44	0.402
DKK1 (pg/mL)*	2051.56 \pm 927.56	3608.22 \pm 2953.12	0.027

β -CTX beta-C-telopeptides of type I collagen (0.26~0.512 ng/mL), DKK1 Dickkopf-related protein 1 (3880.96~6044.21 pg/mL)

sRANKL/OPG (87.12~178.8), Urinary PGE2 (36.4~85.5 ng/mmol creatinine)

Data are expressed as the mean \pm SD or median (interquartile range (IQR)). A value of p are adjusted by height, weight, and age

Boldface indicates statistically significant difference between two groups. * $p < 0.05$; ** $p < 0.01$

HR-pQCT measurement of the distal radius and tibia

HR-pQCT data for PHOAR1 patients, PHOAR2 patients, and HCs are detailed in Table 3.

Comparison between PHOAR1 patients, PHOAR2 patients, and HCs

At the radius, PHOAR1 and PHOAR2 patients had larger total, trabecular and cortical bone cross-sectional areas, and lower total, trabecular and cortical volumetric BMD in comparison to HCs. On the assessment of trabecular bone, PHOAR1 patients showed significantly inferior trabecular microstructure with lower Tb.BV/TV and Tb.N and greater Tb.Sp and Tb.l/N.SD when compared with HCs. SMI was significantly higher in both subtypes of PHO patients than in HCs. On the assessment of cortical bone, all PHOAR1 and PHOAR2 patients had greater Ct.Po than HCs. Regarding FEA, PHOAR1 and PHOAR2 patients showed lower Apparent Young's Modulus than HCs.

At the tibia, total, trabecular, and cortical volumetric BMD was significantly lower, and total and trabecular bone cross-sectional areas were enlarged in all PHOAR1 and PHOAR2 patients when compared with HCs. Ct.Ar increased in PHOAR2 patients, but not in PHOAR1 patients, compared with HCs. On the assessment of trabecular bone, evidence of compromised trabecular integrity was found in PHOAR1 patients with lower Tb.BV/TV, Tb.N, higher trabecular spacing, and a more inhomogeneous trabecular network when compared with HCs. PHOAR2 patients had higher Tb.N and lower Tb.Sp than HCs. SMI was significantly higher in all PHOAR1 and PHOAR2 patients than in HCs. On the assessment of cortical bone, PHOAR1

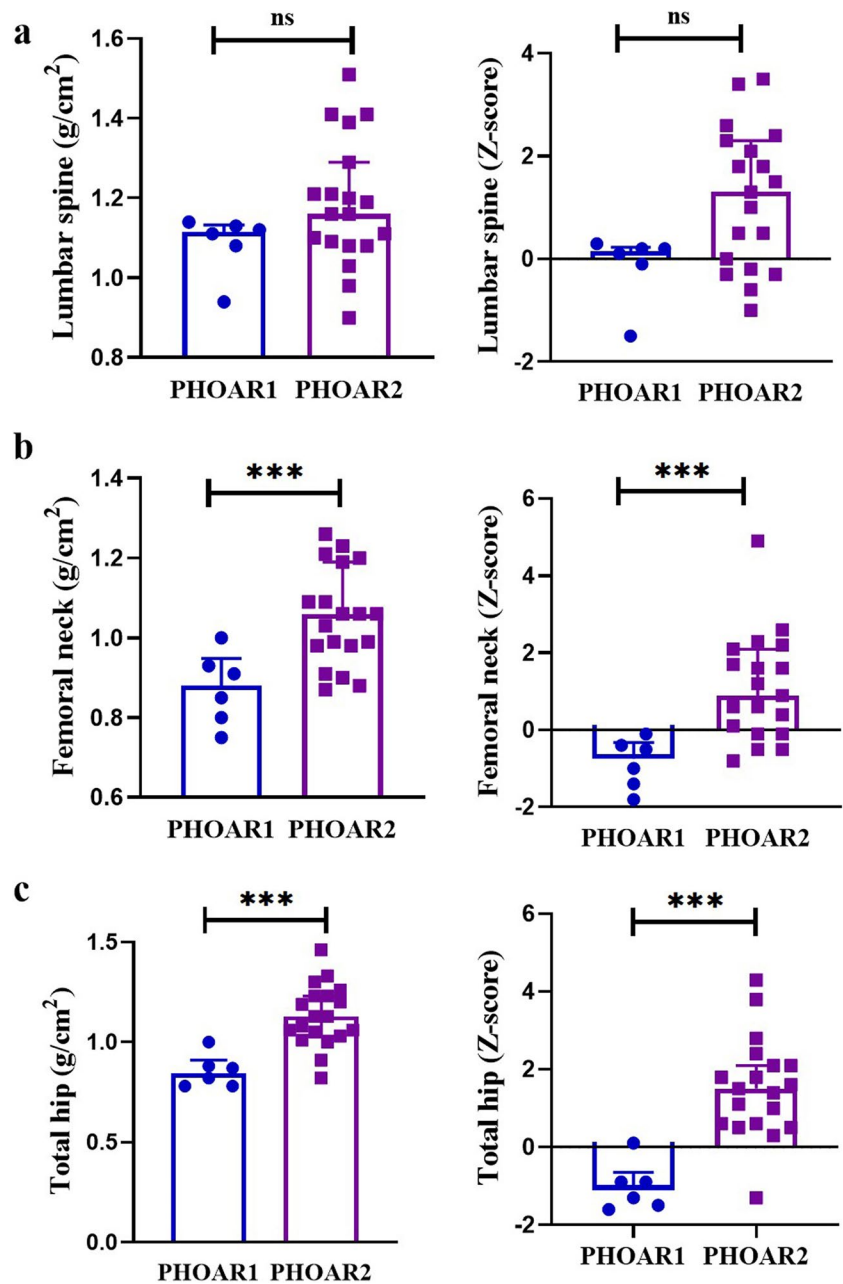
and PHOAR2 patients had increased cortical perimeters. Ct.Th was significantly lower in PHOAR1 patients, and more pores were found in PHOAR2 patients than in HCs. Regarding FEA, the PHOAR1 patients had lower estimated bone strength with lower stiffness, failure load and apparent Young's modulus than HCs. The comparisons in HR-pQCT parameters and biomechanical properties between PHOAR1 patients and HCs and PHOAR2 patients and HCs are presented in Fig. 2a, b.

Comparison between PHOAR1 and PHOAR2 patients

At the radius, a significantly lower Tb.N, greater Tb.Sp, and a more inhomogeneous trabecular network were observed in PHOAR1 patients than in PHOAR2 patients. Almost all of the indices of volumetric BMD, cross-sectional areas, cortical microstructure, and estimated bone strength were comparable between PHOAR1 and PHOAR2 patients, except for Tb.BMD, which was significantly lower in PHOAR1 patients than in PHOAR2 patients.

At the tibia, PHOAR1 patients had significantly lower Tt.BMD and Tb.BMD than PHOAR2 patients. All indices of trabecular microstructure, except for Tb.Th, were significantly inferior in PHOAR1 patients than in PHOAR2 patients, with percentage differences ranging from -41.7% (Tb.BV/TV) to 46.2% (Tb.Sp). The SMI value was significantly higher in PHOAR1 patients, suggesting a more rod-like trabecular network. Ct.Th was, on average, -41.8% lower in PHOAR1 patients than in PHOAR2 patients, and Ct.Po was, on average, -79.5% lower in PHOAR1 patients than in PHOAR2 patients. PHOAR1 patients had lower estimated bone strength, including bone stiffness, failure load, and apparent Young's modulus, than PHOAR2 patients.

Fig. 1 areal bone mineral density (aBMD) at the lumbar spine (a), femoral neck (b), and total hip (c) by DXA in PHOAR1 ($n=6$) and PHOAR2 patients ($n=19$). No significant differences in aBMD L1-4 were found at the lumbar spine (a). aBMD of the femoral neck and total hip were significantly lower in PHOAR1 patients compared with PHOAR2 patients (b, c). Asterisk denotes a significant difference compared with HCs. *** $p < 0.001$



Linear regression for disease features and HR-pQCT parameters

First, we tested whether the disease duration could explain the HR-pQCT parameters. Significantly, correlations were found for the univariate model with Tb.BMD and Tb.N at the radius and tibia as the explained variable. Besides, significant correlations were also found for the univariate model with Tb.Ar and Tb.BV/TV at the tibia as explained variable. Moreover, these effects persisted after adjustment for the type of PHO.

Second, we investigated the predictive effect of biochemical markers on the HR-pQCT parameters. Urinary

PGE2/PGEM were significantly associated to Tb.BMD, Tb.N, and Tb.BV/TV at the radius and tibia in the univariate model and the model adjusted for type of PHO. Additionally, we found significant predictive effects of urinary PGE2/PGEM on biomechanical properties, stiffness, and failure load at the tibia in the univariate model and the model adjusted for type of PHO. DKK1 was significantly associated to Ct.BMD at the radius, but this effect did not persist in the multivariable model. β -CTX was significantly associated to Ct.Ar at the radius and tibia in the univariate model and also after adjustment for type of PHO. Data are shown in Table 4.

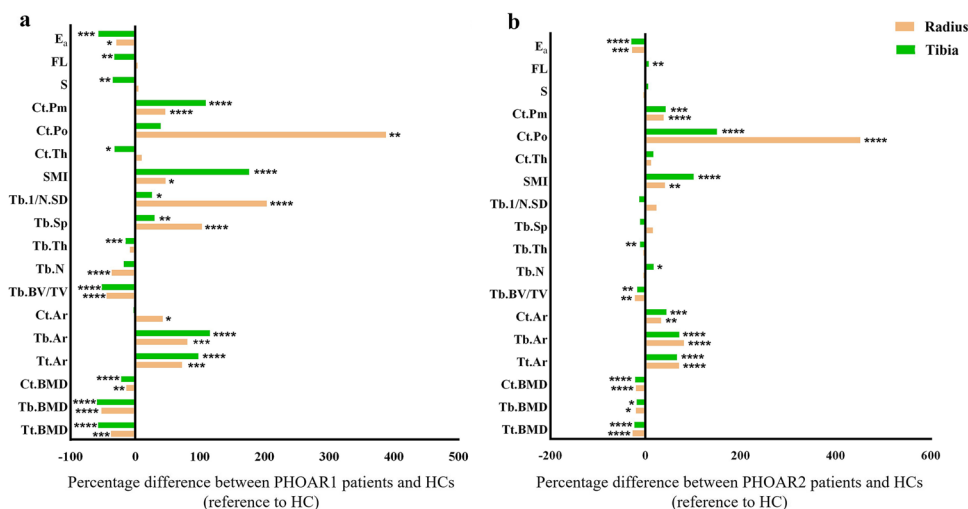
Table 3 HR-pQCT parameters for PHOAR1 patients, PHOAR2 patients, and healthy controls (HCs)

No. of participants	PHOAR1 (n=7) Group 1	PHOAR2 (n=20) Group 2	HCs (n=27) Group 3	p value Group 1 vs. group 3	p value Group 2 vs. group 3	p value Group 1 vs. group 2
<i>Distal radius</i>						
vBMD (mgHA/cm ³)						
Tt.BMD	217.37 ± 66.61	254.27 ± 79.03	347.55 ± 64.99	0.0002	0.0001	0.714
Tb.BMD	87.64 ± 49.26	146.67 ± 47.09	183.76 ± 41.50	0.0001	0.017	0.0016
Ct.BMD	769.34 ± 90.05	713.72 ± 104.81	891.65 ± 57.83	0.002	0.0001	0.371
Cross-sectional geometry (mm ²)						
Tt.Ar	573.7 ± 130.72	566.75 ± 196.82	332.62 ± 63.01	0.0002	0.0001	1.000
Tb.Ar	469.89 ± 125.53	470.55 ± 173.47	259.88 ± 60.15	0.0003	0.0001	1.000
Ct.Ar	109.73 ± 20.76	102.14 ± 44.71	76.89 ± 11.26	0.025	0.010	1.000
Trabecular microstructure						
Tb.BV/TV	0.15 ± 0.06	0.21 ± 0.07	0.27 ± 0.06	0.0001	0.007	0.066
Tb.N (mm ⁻¹)	0.91 ± 0.36	1.37 ± 0.27	1.43 ± 0.21	0.0001	1.000	0.0004
Tb.Th (mm)	0.23 ± 0.02	0.24 ± 0.04	0.25 ± 0.02	0.280	0.723	1.000
Tb.Sp (mm)	1.32 ± 0.69	0.75 ± 0.19	0.65 ± 0.11	0.0001	0.702	0.0001
Tb.1/N.SD (tmm)	0.79 ± 0.63	0.32 ± 0.12	0.26 ± 0.05	0.0001	1.000	0.0001
SMI	1.84 ± 0.31	1.76 ± 0.39	1.25 ± 0.58	0.022	0.005	1.000
Cortical microstructure						
Ct.Th (mm)	1.29 ± 0.23	1.31 ± 0.45	1.17 ± 0.18	1.000	0.363	1.000
Ct.Po (%)	2.83 ± 1.54	3.20 ± 2.19	0.58 ± 0.32	0.001	0.0001	1.000
Ct.Pm (mm)	112.21 ± 30.23	105.65 ± 29.37	76.44 ± 7.71	0.0005	0.0001	1.000
Biomechanical indices						
S (kN/mm)	96.78 ± 26.53	92.75 ± 40.62	92.18 ± 16.41	1.000	1.000	1.000
FL (kN)	5.23 ± 1.32	4.92 ± 2.16	5.04 ± 0.85	1.000	1.000	1.000
E _a (kN/mm ²)	1.424 ± 0.490	1.456 ± 0.541	2.015 ± 0.392	0.013	0.001	1.000
<i>Distal tibia</i>						
vBMD (mgHA/cm ³)						
Tt.BMD	141.97 ± 55.87	257.19 ± 58.60	334.71 ± 61.10	0.0001	0.0001	0.0003
Tb.BMD	79.02 ± 38.56	157.72 ± 37.68	193.42 ± 43.06	0.0001	0.011	0.0004
Ct.BMD	719.23 ± 86.71	724.68 ± 64.17	921.18 ± 37.25	0.0001	0.0001	1.000
Cross-sectional geometry (mm ²)						
Tt.Ar	1534.73 ± 204.07	1290.34 ± 343.48	776.88 ± 130.57	0.0001	0.0001	0.091
Tb.Ar	1363.98 ± 172.10	1081.62 ± 317.56	632.31 ± 133.13	0.0001	0.0001	0.024
Ct.Ar	151.95 ± 56.08	216.74 ± 78.10	150.26 ± 23.87	1.000	0.0002	0.033
Trabecular microstructure						
Tb.BV/TV	0.14 ± 0.05	0.24 ± 0.06	0.29 ± 0.06	0.0001	0.010	0.002
Tb.N (mm ⁻¹)	1.11 ± 0.26	1.58 ± 0.23	1.35 ± 0.27	0.119	0.011	0.001
Tb.Th (mm)	0.23 ± 0.01	0.24 ± 0.03	0.27 ± 0.03	0.001	0.002	0.545
Tb.Sp (mm)	0.95 ± 0.23	0.65 ± 0.11	0.73 ± 0.15	0.004	0.164	0.0001
Tb.1/N.SD (tmm)	0.39 ± 0.09	0.27 ± 0.05	0.31 ± 0.07	0.016	0.265	0.001
SMI	2.10 ± 0.27	1.53 ± 0.56	0.76 ± 0.60	0.0001	0.0001	0.105
Cortical microstructure						
Ct.Th (mm)	1.10 ± 0.36	1.89 ± 0.56	1.62 ± 0.31	0.023	0.091	0.001
Ct.Po (%)	2.83 ± 1.19	5.08 ± 2.58	2.03 ± 0.94	0.918	0.0001	0.022
Ct.Pm (mm)	227.68 ± 126.80	154.86 ± 30.24	108.73 ± 9.10	0.0001	0.002	0.002
Biomechanical indices						
S (kN/mm)	163.87 ± 73.47	265.89 ± 69.58	251.21 ± 47.12	0.006	1.000	0.002
FL (kN)	9.13 ± 4.06	14.44 ± 3.63	13.50 ± 2.43	0.009	0.972	0.002
E _a (kN/mm ²)	1.216 ± 0.304	2.002 ± 0.577	2.844 ± 0.570	0.0001	0.0001	0.012

BMD bone mineral density, Tb trabecular, Ct cortical, Ar area, Tb.BV/TV trabecular bone volume fraction, N number, Th thickness, Sp separation, SMI structure model index, Po porosity, Pm perimeter, Tb.1/N.SD inhomogeneity of trabecular network, S stiffness, FL estimated failure load, E_a apparent Young’s modulus

Data are expressed as the mean ± SD. Groups were compared using ANOVA with Bonferroni-correct pairwise comparisons p < 0.05 is considered statistically significant indicated in bold

Fig. 2 Differences in mean of bone parameters between PHOAR1 patients and HCs (a) or between PHOAR2 patients with HCs (b) expressed as percentage. Orange bars represent radius and green bars represent tibia. Asterisk denotes a significant difference compared with HCs. * $p < 0.05$, ** $p < 0.01$, *** $p < 0.001$, and **** $p < 0.0001$



Discussion

This study used HR-pQCT to assess bone structural parameters and estimated bone biomechanics of the appendicular skeleton in PHOAR1 and PHOAR2 patients. This study represents a continuation of our previous report that described alterations in bone quality in PHO patients [10]. While the previous study mainly focused on evaluating bone microarchitecture at weight-bearing distal tibia in PHO patients, the current study involved the aim of comparing bone microarchitecture and bone strength at both non-weight-bearing distal radius and weight-bearing distal tibia sites between PHOAR1 and PHOAR2 patients. Moreover, for the first time, this study evaluated the influence of Wnt signaling (DKK1) on alterations in bone quality in patients with the two subtypes of PHO.

Cortical width is determined by modeling the endocortical and periosteal surface [18]. Periosteosis is a typical imaging feature of PHO patients. In the current study, all PHOAR1 and PHOAR2 patients showed distinct periosteosis imaging features with periosteosis in the cortex of long bones. Bone microarchitecture evaluation revealed higher Ct.Ar and Ct.Pm but lower Ct.BMD in PHOAR1 and PHOAR2 patients than in HCs, consistent with our previous PHO study, indicating “trabecularization” of cortical bone and excessive accumulation of unmineralized osteoid in the cortical compartment [10]. Subgroup comparison analysis of PHOAR1 and PHOAR2 patients revealed higher Ct.Pm but lower Ct.Ar at the tibia in PHOAR1 patients than PHOAR2 patients, indicating more irregular cortical bone formation of PHOAR1 at the tibia.

Notably, the present study found that DKK1 was significantly associated to Ct.BMD at the radius and the association was affected by the type of PHO. Regarding DKK1 level, the PHOAR2 patients showed higher level than the PHOAR1 patients. Urinary PGE2/PGEM level was higher in PHOAR1 patients than in PHOAR2 patients. These data corroborate previous studies showing a role for high PGE2 level influencing

the Wnt signaling pathway and inhibition of DKK1 secretion [19]. HR-pQCT measurement revealed a higher Ct.BMD in PHOAR1 patients than in PHOAR2 patients. The observation of high DKK1 level and decreased Ct.BMD in PHOAR2 patients suggesting DKK1 could be a biomarker of compromised cortical bone. Moreover, bone resorption marker, β -CTX, showed significantly associated to Ct.Ar at the radius and tibia in the univariate model. In the current study, β -CTX level increased in PHOAR1 and PHOAR2 patients. Both PHOAR1 and PHOAR2 patients had larger Ct.Ar than in HCs. The observation of elevated level of β -CTX and lower DKK1 level in PHO patients reflected imbalances in bone remodeling, which might be another reason for the discrepancy in cortical bone microstructure (larger Ct.Ar and lower Ct.BMD) in PHO patients.

Apart from abnormal findings in the cortical compartment, abnormal bone microarchitecture in the trabecular compartment was also noted in PHOAR1 and PHOAR2 patients. In the weight-bearing tibia, the alterations in trabecular microstructure in PHOAR1 and PHOAR2 patients were in opposite directions. PHOAR1 patients were associated with significant deficits in the trabecular compartment, resulting in lower estimated bone strength at the weight-bearing tibia than HCs. The findings in PHOAR1 patients indicated a disproportionate loss of trabecular bone. However, in PHOAR2 patients, the trabecular bone microstructure improved with a higher Tb.N and narrower Tb.Sp at the weight-bearing tibia than in HCs, indicating enhanced trabecular bone formation in PHOAR2 patients. The underlying cause for this discrepancy was unclear. One of the reasons was probably the impact of the skeletal anabolism of PGE2. Significant relations between urinary PGE2/PGEM and trabecular bone microstructure were found in the present study, suggesting that urinary PGE2/PGEM level could be a predicted marker for reflecting the trabecular changes of PHO patients. In the current study, the urinary PGE2/PGEM ratio in PHOAR1 patients was significantly higher than that in PHOAR2 patients. *SLCO2A1*, the

Table 4 Linear regression models with disease duration and biochemical markers as independent variable and selected HR-pQCT parameters as explained variable in all PHO patients

	Disease duration			Urinary PGE2/PGE1			Dkk1			β-CTX						
	Univariate		Adjusted	Univariate		Adjusted	Univariate		Adjusted	Univariate		Adjusted				
	R ²	p value	R ²	R ²	p value	R ²	R ²	p value	R ²	R ²	p value	R ²	p value			
<i>Distal radius</i>																
Tb.BMD	0.116	0.046	0.179	0.036	0.288	0.005	0.338	0.009	0.036	0.389	0.421	0.004	0.025	0.434	0.242	0.036
Ct.BMD	0.041	0.311	0.059	0.483	0.076	0.174	0.079	0.389	0.208	0.029	0.214	0.090	0.115	0.084	0.136	0.173
Tb.Ar	0.036	0.346	0.103	0.271	0.001	0.868	0.002	0.978	0.002	0.846	0.003	0.971	0.001	0.921	0.001	0.968
Ct.Ar	0.134	0.061	0.259	0.027	0.015	0.549	0.051	0.547	0.040	0.358	0.041	0.659	0.309	0.003	0.317	0.010
Tb.BV/TV	0.105	0.099	0.168	0.110	0.197	0.023	0.233	0.047	0.030	0.430	0.329	0.018	0.009	0.644	0.169	0.108
Tb.N	0.190	0.023	0.339	0.007	0.414	0.001	0.476	0.001	0.009	0.671	0.435	0.003	0.075	0.168	0.347	0.006
Ct.Po	0.006	0.702	0.065	0.444	0.040	0.325	0.045	0.592	0.006	0.718	0.007	0.928	0.002	0.815	0.012	0.860
S	0.062	0.231	0.124	0.233	0.015	0.571	0.030	0.727	0.001	0.979	0.002	0.849	0.121	0.088	0.124	0.233
FL	0.072	0.196	0.128	0.221	0.010	0.638	0.029	0.738	0.001	0.947	0.001	0.919	0.130	0.077	0.131	0.214
<i>Distal tibia</i>																
Tb.BMD	0.331	0.002	0.460	0.001	0.290	0.006	0.456	0.001	0.090	0.174	0.654	0.001	0.014	0.567	0.459	0.001
Ct.BMD	0.029	0.408	0.054	0.528	0.011	0.625	0.057	0.526	0.053	0.303	0.087	0.423	0.030	0.396	0.038	0.643
Tb.Ar	0.296	0.004	0.300	0.017	0.031	0.401	0.180	0.112	0.005	0.756	0.148	0.219	0.008	0.672	0.193	0.085
Ct.Ar	0.001	0.914	0.368	0.005	0.165	0.044	0.186	0.104	0.009	0.668	0.238	0.075	0.171	0.036	0.415	0.002
Tb.BV/TV	0.257	0.008	0.376	0.004	0.258	0.010	0.379	0.005	0.107	0.137	0.561	0.001	0.004	0.748	0.386	0.004
Tb.N	0.228	0.014	0.421	0.002	0.245	0.012	0.428	0.002	0.079	0.207	0.525	0.001	0.092	0.131	0.435	0.001
Ct.Po	0.001	0.970	0.374	0.005	0.151	0.055	0.172	0.125	0.051	0.313	0.165	0.181	0.012	0.590	0.200	0.077
S	0.035	0.380	0.450	0.002	0.287	0.008	0.344	0.015	0.006	0.747	0.437	0.006	0.103	0.127	0.536	0.001
FL	0.032	0.401	0.447	0.002	0.284	0.009	0.339	0.016	0.005	0.758	0.432	0.006	0.101	0.130	0.524	0.001

BMD bone mineral density, Tb trabecular, Ct cortical, Ar area, Tb.BV/TV trabecular bone volume fraction, N number, Po porosity, S stiffness, FL estimated failure load, R² coefficient of determination

p < 0.05 is considered statistically significant indicated in bold

pathogenic gene for PHOAR2, is responsible for transporting extracellular PGE2 into the cell, functions intracellularly, and is subsequently degraded by 15-PGDH, which *HPGD* encodes, the causative gene for PHOAR1, in the cell into PGEM [4, 5]. The observation of a significantly higher PGE2/PGEM ratio in PHOAR1 patients suggested that PHOAR1 patients had more active PGE2 accumulating and functioning intracellularly. Additionally, the mean disease duration of PHOAR1 patients in this study was 28 years, which was much longer than that of PHOAR2 patients. All the above results indicated that in PHOAR1 patients, more active PGE2 accumulated in the cells and acted for a long time. Association analysis revealed significant correlations for disease duration with trabecular compartment including Tb.BMD, Tb.N, Tb.Ar, and Tb.BV/TV. Tian et al. in animal studies [20] found that continuous PGE2 treatment via the Infu-DiskTM pump decreased cancellous bone mass and architecture. Intermittent PGE2 administration by subcutaneous injection for the same days increased cancellous bone architecture, reflecting that bone gain or bone loss largely depended on the route of PGE2 administration and the concentration of PGE2. Therefore, the time- and concentration-dependent PGE2 skeletal anabolism might in theory explain the discrepancy in trabecular bone microstructure between PHOAR1 and PHOAR2 patients.

Trabecular formation primarily occurs during endochondral ossification at the growth plate-metaphyseal bone interface, followed by refinement of the structure by modeling and remodeling [21]. Bone remodeling is a maintenance process entailing the sequential activity of osteoclasts and osteoblasts on the same surface of the trabeculae [22]. Inferior trabecular bone microstructure of PHOAR1 patients at the weight-bearing tibia indicates negative trabecular bone balance, with the increase in bone resorption exceeding the increase in bone formation. In

contrast, the larger Tb.Ar, higher Tb.N, and narrower Tb.Sp at the weight-bearing tibia in PHOAR2 patients reflect numerous new bone formations in the trabecular compartment. Conversely, lower Tb.Th and Tb.BV/TV found in PHOAR2 patients suggested enhanced bone resorption. The estimated bone strength of PHOAR2 patients was normal or slightly high. The increased bone formation and bone resorption but normal or slightly high bone strength in PHOAR2 patients might be explained by the following reasons: (1) positive trabecular bone balance with an imbalance of resorption and formation in favor of formation and (2) the newly formed bone in the trabecular compartment might be less mineralized and haphazardly organized woven bone. Additionally, higher Tb.N and reduced Tb.Sp were observed in PHOAR2 patients at the weight-bearing tibia but not at the non-weight-bearing radius. Tang et al. found a synergistic effect between minor overloading and PGE2 levels in stimulating bone formation [23]. The significant differences in trabecular bone microstructure involvement of weight-bearing and non-weight-bearing skeletal sites could result from the synergistic effect between mechanical loading and PGE2 levels.

There were some limitations to this study. First, Xu et al. revealed that biallelic mutations or monoallelic mutations in *SLCO2A1* cause PHOAR2, and PHOAD (PHO autosomal dominant) is the pathogenesis of PHO [24]. However, due to the small sample size, the comparison of PHOAR2 and PHOAD in clinical features, biochemical markers, and bone microstructure was not involved in this study. Second, periosteosis and trabecularization of the cortical bone in PHOAR1 and PHOAR2 patients might impact the evaluation of HR-pQCT images. Additionally, the FEA solver in this study assumed fixed, homogeneous material properties that were likely not true, especially for PHOAR1 and PHOAR2 patients. Third, HR-pQCT only allowed investigation at the peripheral site and

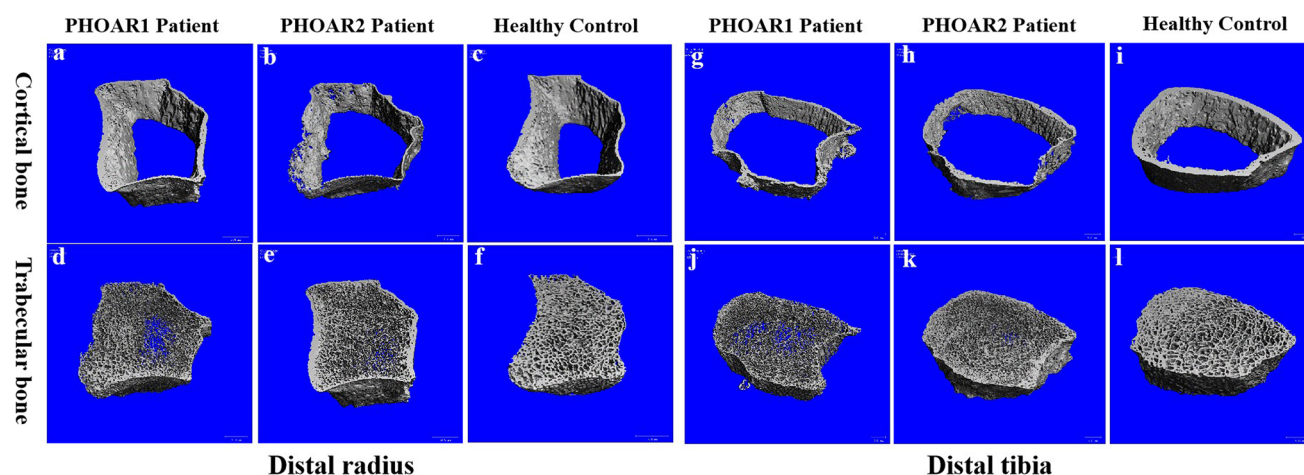


Fig. 3 3D visualization of cortical bone and trabecular bone in representative PHOAR1 patient (a, d, g, j), PHOAR2 patient (b, e, h, k), and healthy control (c, f, i, l) in distal radius and tibia, respectively.

The enlarged bone geometry and compromised cortical bone compartment evident in both PHOAR1 and PHOAR2 patients. The compromised trabecular compartment is apparent in PHOAR1 patients

did not provide a direct measure of bone quality at the hip and spine, which are more common sites of fragility fracture. Liu et al. reported that the HR-pQCT measurement at the radius correlated well with the measurement by central QCT at the spine [25]. The radius was a non-weight-bearing region, and HR-pQCT measurement at the distal radius was unlikely to be significantly affected by body weight and BMI. Bone density, microarchitecture, and mechanical properties at the distal radius could reflect the mechanical competence of the spine and hip of PHOAR1 and PHOAR2 patients [25]. Finally, remodeling mechanisms in PHOAR1 and PHOAR2 patients would have required a biopsy, which was not undertaken in this study.

In summary, this study utilized HR-pQCT to investigate alterations in density, geometrical, microstructural, and biomechanical competence at the distal radius and tibia in patients with the two subtypes of PHO. We found that PHOAR1 and PHOAR2 patients had distinctively larger bone geometry and substantially lower volumetric BMD at the radius and tibia compared with HCs. Trabecular bone microstructure was altered differently in PHOAR1 and PHOAR2 patients at the distal tibia. PHOAR1 patients showed compromised trabecular microstructure than HCs. However, the trabecular microstructure tends to be improved in PHOAR2 patients (Fig. 3). Alterations in bone microstructure in PHOAR1 patients translated into lower estimated bone strength. Conversely, PHOAR2 patients showed preserved or slightly high estimated bone strength. For the first time, the study revealed the bone microstructural differences between the two subtypes of PHO and revealed that PHOAR1 patients had more inferior bone microstructure and bone strength than PHOAR2 patients. All the findings expanded our understanding of the bone pathophysiology in PHOAR1 and PHOAR2 patients and filled the gap in PHO classification.

Supplementary Information The online version contains supplementary material available at <https://doi.org/10.1007/s00198-023-06784-w>.

Acknowledgements We would like to thank the patients or health subjects for consenting to participate in this study.

Author contribution Prof. Weibo Xia and Prof. Ling Qin were responsible for study design and manuscript editing. Dr. Qianqian Pang performed the study and prepared the first draft of the paper. Ms. Qianqian Pang, Ms. Yuping Xu, and Dr. Ruoxi Liao contributed to the experimental work. Dr. Qianqian Pang and Ms. Yuping Xu were responsible for statistical analysis of the data. Ms. Li Zhang contributed to the imaging working. Prof. Mei Li, Prof. Ou Wang, Prof. Yan Jiang, Prof. Xiaoping Xing, Dr. Ye Li, Dr. Yue Chi, and Dr. Xuan Qi contributed in revising the paper critically for intellectual content. All listed authors approved the final version of the submitted manuscript.

Funding This study was supported by the National Key R&D Program of China (2018YFA0800801, 2021YFC2501700), CAMS Innovation Fund for Medical Sciences (CIFMS-2021-I2M-1-002, 2020-I2M-C&T-B-016), the National Natural Science Foundation of China (81970757, 81900798), and grant from Peking Union Medical College Hospital (ZC201904197, 2017PT32020, and 2018PT32001).

Data availability The datasets used and/or analyzed during the current study are available from the corresponding author on reasonable request.

Declarations

Conflict of interest None.

Open Access This article is licensed under a Creative Commons Attribution-NonCommercial 4.0 International License, which permits any non-commercial use, sharing, adaptation, distribution and reproduction in any medium or format, as long as you give appropriate credit to the original author(s) and the source, provide a link to the Creative Commons licence, and indicate if changes were made. The images or other third party material in this article are included in the article's Creative Commons licence, unless indicated otherwise in a credit line to the material. If material is not included in the article's Creative Commons licence and your intended use is not permitted by statutory regulation or exceeds the permitted use, you will need to obtain permission directly from the copyright holder. To view a copy of this licence, visit <http://creativecommons.org/licenses/by-nc/4.0/>.

References

1. Marrie TJ, Brown N (2007) Clubbing of the digits. *Am J Med* 120:940–941
2. Uppal S, Diggle CP, Carr IM, Fishwick CW, Ahmed M, Ibrahim GH, Helliwell PS, Latos-Bielenska A, Phillips SE, Markham AF, Bennett CP, Bonthron DT (2008) Mutations in 15-hydroxyprostaglandin dehydrogenase cause primary hypertrophic osteoarthropathy. *Nat Genet* 40:789–793
3. Zhang Z, Xia W, He J, Zhang Z, Ke Y, Yue H, Wang C, Zhang H, Gu J, Hu W, Fu W, Hu Y, Li M, Liu Y (2012) Exome sequencing identifies *SLCO2A1* mutations as a cause of primary hypertrophic osteoarthropathy. *Am J Hum Genet* 90:125–132
4. Ensor CM, Tai HH (1995) 15-Hydroxyprostaglandin dehydrogenase. *J Lipid Mediat Cell Signal* 12:313–319
5. Lu R, Kanai N, Bao Y, Schuster VL (1996) Cloning, in vitro expression, and tissue distribution of a human prostaglandin transporter cDNA(hPGT). *J Clin Invest* 98:1142–1149
6. Li SS, He JW, Fu WZ, Liu YJ, Hu YQ, Zhang ZL (2017) Clinical, biochemical, and genetic features of 41 Han Chinese families with primary hypertrophic osteoarthropathy, and their therapeutic response to etoricoxib: results from a six-month prospective clinical intervention. *J Bone Miner Res* 32:1659–1666
7. Hou Y, Lin Y, Qi X, Yuan L, Liao R, Pang Q, Cui L, Jiang Y, Wang O, Li M, Dong J, Xia W (2018) Identification of mutations in the prostaglandin transporter gene *SLCO2A1* and phenotypic comparison between two subtypes of primary hypertrophic osteoarthropathy (PHO): A single-center study. *Bone* 106:96–102
8. Wittenberg RH, Willburger RE, Kleemeyer KS, Peskar BA (1993) In vitro release of prostaglandins and leukotrienes from synovial tissue, cartilage, and bone in degenerative joint diseases. *Arthritis Rheum* 36:1444–1450
9. Pang Q, Xu Y, Qi X, Huang L, Hung VW, Xu J, Liao R, Hou Y, Jiang Y, Yu W, Wang O, Li M, Xing X, Xia W, Qin L (2020) Impaired bone microarchitecture in distal interphalangeal joints in patients with primary hypertrophic osteoarthropathy assessed by high-resolution peripheral quantitative computed tomography. *Osteoporos Int* 31:153–164
10. Pang Q, Xu Y, Huang L, Li Y, Lin Y, Hou Y, Hung VW, Qi X, Ni X, Li M, Jiang Y, Wang O, Xing X, Qin L, Xia W (2022) Bone

- geometry, density, microstructure, and biomechanical properties in the distal tibia in patients with primary hypertrophic osteoarthropathy assessed by second-generation high-resolution peripheral quantitative computed tomography. *J Bone Miner Res* 37:484–493
11. McDonald MM, Morse A, Schindeler A, Mikulec K, Peacock L, Cheng T, Bohn J, Lee L, Baldock PA, Croucher PI, Tam P, Little DG (2018) Homozygous *Dkk1* knockout mice exhibit high bone mass phenotype due to increased bone formation. *Calcif Tissue Int* 102:105–116
 12. MacDonald BT, Joiner DM, Oyserman SM, Sharma P, Goldstein SA, He X, Hauschka PV (2007) Bone mass is inversely proportional to *Dkk1* levels in mice. *Bone* 41:331–339
 13. Yu F, Xu Y, Hou Y, Lin Y, Jiajue R, Jiang Y, Wang O, Li M, Xing X, Zhang L, Qin L, Hsieh E, Xia W (2020) Age-, site-, and sex-specific normative centile curves for HR-pQCT-derived microarchitectural and bone strength parameters in a Chinese mainland population. *J Bone Miner Res* 35:2159–2170
 14. Pauchard Y, Liphardt AM, Macdonald HM, Hanley DA, Boyd SK (2012) Quality control for bone quality parameters affected by subject motion in high-resolution peripheral quantitative computed tomography. *Bone* 50:1304–1310
 15. Whittier DE, Boyd SK, Burghardt AJ, Paccou J, Ghasem-Zadeh A, Chapurlat R, Engelke K, Bouxsein ML (2020) Guidelines for the assessment of bone density and microarchitecture in vivo using high-resolution peripheral quantitative computed tomography. *Osteoporos Int* 31:1607–1627
 16. Zhu TY, Griffith JF, Qin L, Hung VW, Fong TN, Au SK, Tang XL, Kwok AW, Leung PC, Li EK, Tam LS (2013) Structure and strength of the distal radius in female patients with rheumatoid arthritis: a case-control study. *J Bone Miner Res* 28:794–806
 17. Zhu TY, Griffith JF, Qin L, Hung VW, Fong TN, Au SK, Li M, Lam YY, Wong CK, Kwok AW, Leung PC, Li EK, Tam LS (2014) Alterations of bone density, microstructure, and strength of the distal radius in male patients with rheumatoid arthritis: a case-control study with HR-pQCT. *J Bone Miner Res* 29:2118–2129
 18. Parfitt AM, Travers R, Rauch F, Glorieux FH (2000) Structural and cellular changes during bone growth in healthy children. *Bone* 27:487–494
 19. Kabashima K, Sakabe J, Yoshiki R, Tabata Y, Kohno K, Tokura Y (2010) Involvement of Wnt signaling in dermal fibroblasts. *Am J Pathol* 176:721–732
 20. Tian XY, Zhang Q, Zhao R, Setterberg RB, Zeng QQ, Ma YF, Jee WS (2007) Continuous infusion of PGE₂ is catabolic with a negative bone balance on both cancellous and cortical bone in rats. *J Musculoskelet Neuronal Interact* 7:372–381
 21. Yu WS, Chan KY, Yu FW, Ng BK, Lee KM, Qin L, Lam TP, Cheng JC (2014) Bone structural and mechanical indices in adolescent idiopathic scoliosis evaluated by high-resolution peripheral quantitative computed tomography (HR-pQCT). *Bone* 61:109–115
 22. Shanbhogue VV, Hansen S, Folkestad L, Brixen K, Beck-Nielsen SS (2015) Bone geometry, volumetric density, microarchitecture, and estimated bone strength assessed by HR-pQCT in adult patients with hypophosphatemic rickets. *J Bone Miner Res* 30:176–183
 23. Tang LY, Cullen DM, Yee JA, Jee WS, Kimmel DB (1997) Prostaglandin E₂ increases the skeletal response to mechanical loading. *J Bone Miner Res* 12:276–282
 24. Xu Y, Zhang Z, Yue H, Li S, Zhang Z (2021) Monoallelic mutations in *SLCO2A1* cause autosomal dominant primary hypertrophic osteoarthropathy. *J Bone Miner Res* 36:1459–1468
 25. Liu XS, Cohen A, Shane E, Yin PT, Stein EM, Rogers H, Kokolus SL, McMahon DJ, Lappe JM, Recker RR, Lang T, Guo XE (2010) Bone density, geometry, microstructure, and stiffness: relationships between peripheral and central skeletal sites assessed by DXA, HR-pQCT, and cQCT in premenopausal women. *J Bone Miner Res* 25:2229–2238

Publisher's note Springer Nature remains neutral with regard to jurisdictional claims in published maps and institutional affiliations.